Seismic anisotropy inferred from direct S-waves derived splitting measurements and its geodynamic implications beneath southeastern Tibetan Plateau

Ashwani Kant Tiwari[1], Arun Singh[1], Tuna Eken[2], Nitin Grewal[1], and Chandrani Singh[1]

[1]Department of Geology and Geophysics, , Indian Institute of Technology Kharagpur, India
[2]Department of Geophysical Engineering, , Istanbul Technical University, Turkey

Correspondence to: Arun Singh (arun@gg.iitkgp.ernet.in)

Abstract. The present study deals with detecting seismic anisotropy parameters beneath southeastern Tibet near Namche Barwa Mountain using splitting of the direct S-waves. We employed the reference station technique to remove the effects of source side anisotropy. Seismic anisotropy parameters, splitting time delay and fast polarization directions were estimated through analyses on a total of 501 splitting measurements obtained from direct-S waves from 25 earthquakes (>5.5 magnitude) that were recorded at 42 stations of Namchebarwa seismic network. We observed a large variation in time delays ranging from 0.64 to 1.68 s but in most cases it is more than 1 s, which suggests for a highly anisotropic lithospheric mantle in the region. A comparison between direct S- and SKS-derived splitting parameters generally shows a close similarity although some discrepancies exist where null or negligible anisotropy is reported earlier using SKS. The seismic stations with hitherto null or negligible anisotropy are now supplemented with new measurements with clear anisotropic signatures. Our analyses indicate a sharp change in lateral variations of fast polarization directions (FPDs) from consistent ENE-SSW or E-W to NW-SE direction at the southeastern edge of Tibet. Comparison of the FPDs with global positioning system (GPS) measurements, absolute plate motion (APM) directions and surface geological features signify that the observed anisotropy and hence inferred deformation patterns are not only due to asthenospheric dynamics but it is a combination of lithospheric deformation and sub-lithospheric (asthenospheric) mantle dynamics. Splitting measurement using direct-S waves proves their utility to supplement the anisotropic measurements in the study region and fills the missing links that remain rather illusive due to lack of SKS measurements.

1 Introduction

The Tibetan plateau has a long history of deformation since 50 million years (e.g., Rowley and Currie, 2006; Henderson et al., 2011). Reliability of seismic anisotropy measurements in the context of the tectonics, coupling/decoupling of the crust-lithospheric mantle, multi-layered anisotropic modeling, and active seismicity in relation to the deformation mechanisms are challenging problems to understand the type of deformation and possible flow patterns and are still a matter of debate in understanding the formation process and future challenges of this active region. Seismic anisotropy is an important tool to decipher the deformation and flow pattern of any tectonic or stable region and used to explain the formation mechanism of that

region. Lattice preferred orientation (LPO) of the olivine mineral in the mantle as a result of plate interactions controlled by various geodynamic processes are the main cause for the shear wave splitting observations on the teleseismic S and SKS waves. Deformation in the upper mantle generally takes place through two processes namely diffusion and dislocation creep under the favorable conditions. Dislocation creep process, which is the creeping motion of crystal dislocation, are considered to be the

5   main cause for the developed anisotropy (Karato, 1987; Nicolas and Christensen, 1987; Karato and Wu, 1993; Mainprice et al., 2000). It is caused either by high stress condition or large grain size or both but the nonlinear increase in the strain rate are independent of the grain size (Karato and Wu, 1993). This type of deformation is generally expected to occur at a depth range less than 400km (e.g., Karato, 1984, 1987) and hence LPO development and observed anisotropy mainly represents upper 400 km depth (Becker and Faccenna, 2011).

10   Several observations on seismic anisotropy have greatly contributed to elucidating these deformation patterns in relation to the past and present geodynamic activities of the region. Generally speaking, SKS splitting analyses are known to be the most diagnostic, quick, and well-established way of detection and quantification of possible signs of seismic anisotropy. The most prominent feature of the SKS phase is that they do not propagate as S-wave in the liquid outer core and refract from P into only SV (radial) component when entering the mantle of receiver-side region. Hence recorded SKS phase at the surface do

15   not pose any influence of the source side anisotropy (e.g., Christensen, 1966; Keith and Crampin, 1977; Ando, 1984; Fukao, 1984; Vinnik et al., 1984, 1992; Kind et al., 1985; Silver and Chan, 1988, 1991; McNamara et al., 1994; Kaneshima and Silver, 1995). The main disadvantage of using SKS phase in splitting measurements is that finding good-quality observations is restricted to several parameters, i.e., epicentral distance and propagation direction of the event in most cases thus and need to be supplemented with other waves (e.g. ScS and direct-S) that can provide a better azimuthal coverage. However, employing

20   such additional waves may introduce the contamination of shear signal due to the anisotropy dominant nearby the source-side.

Splitting of shear waves is similar to the birefringence phenomena in optics. Shear waves split into fast and slow components when they pass through an anisotropic media. In this case we obtain the elliptical particle motion. If the anisotropy is only cause of splitting then the observed shear wave (fast or slow) can be rotated in such a way that two very similar phases are seen apart from scaling and time delay between them (Eken and Tilmann, 2014). Resultant splitting parameters ϕ and δt imply the rotation

25   angle in relation to the flow direction and shearing or extension at a particular depth, and to the strength and thickness of the anisotropic layer, respectively. Splitting measurements from the Himalaya-Tibet collision zone have long been explained using vertical transverse models assuming single homogeneous layer with horizontal axis of the symmetry (e.g., McNamara et al., 1994; Chen et al., 2010; Sol et al., 2007; Herquel et al., 1995; Hirn et al., 1995; Lavé et al., 1996; Sandvol et al., 1997; Huang et al., 2000; Lev et al., 2006; Wang et al., 2008; Fu et al., 2008; Sato et al., 2012). Any single hypothesis is not enough to explain

30   the observed splitting parameters (Bormann et al., 1996; Savage, 1999; Fouch et al., 2000; Fouch and Rondenay, 2006).

The use of direct-S waves of the earthquakes at teleseismic distance ranges (30-90°) can provide sufficient measurements with good azimuthal distribution of splitting parameters in establishing a robust and coherent database. However the major problem in including direct S-waves into splitting measurements is the contamination of the S-wave signals due to the influence of anisotropic structures existing within the source-side region. Eken and Tilmann (2014) have recently shown that this problem

35   can be overcome using an array-based approach (Reference Station Technique in which the source side anisotropy could be

neglected by searching for optimum splitting parameters resulting in the minimum difference between the S-wave signals corrected for receiver-side anisotropy beneath the reference and target stations. Signals used for that comparison are that of the reference station previously corrected for known reference receiver-side anisotropy and of the target station whose receiver-side splitting parameters are desired to be estimated. In this technique we utilize seismic anisotropy parameters, which were
5   previously inferred from the SKS measurements by Sol et al. (2007) as the reference knowledge of the receiver-side anisotropy beneath the reference station. The Reference Station Technique has been earlier successfully tested through both synthetic and observed data collected along the northeastern and southwestern parts of the Tibetan Plateau (Eken and Tilmann, 2014; Singh et al., 2016). Present study focuses on the southeast part of the Tibet near Namche Barwa (Figure 1). Study region is located between and around the Indus-Tsangpo Suture Zone (ITSZ) and Bangong-Nuijiang Suture Zone (BNSZ). Our major
10   motivation is to find out the S-wave derived seismic anisotropic parameters that may have a potential link to current tectonic setting and deformation history with the help of a correlative analysis of resultant anisotropy observations with Absolute Plate Motion (APM) directions, GPS measurements and the structural and topographic features. Our study contradicts the isotropic nature of the isotropic lithospheric mantle and adds new constraints in understanding the types of deformation and their causes in the region.

15 2   Tectonics of the region

The formation of Tibetan plateau and the Himalayan mountain belts are due to collision and post collision processes of the Indian and Eurasian plates since 50 million years ago (Argand, 1924; Garzanti and Van Haver, 1988; Molnar and Tapponnier, 1975; Yin and Harrison, 2000; Royden et al., 2008). Underthrusting of the Indian lithosphere beneath the Eurasian lithosphere is the main responsible reason for the formation of the Himalayan and Karakorum ranges (Nelson et al., 1996; Kumar et al.,
20   2006; Tseng et al., 2009) along with the formation of the Central Tibetan region (Argand, 1924; Nelson et al., 1996; Li et al., 2008). Understanding the development of the northern and eastern Tibetan plateau region are a big challenge (Karplus et al., 2011; Royden et al., 2008). McKenzie and Priestley (2008) discuss the development of the northern Tibetan lithosphere as an accreted one. Royden et al. (2008) argued that the Tibetan plateau has been evolved due to the subduction of Indian lithosphere beneath Eurasia, which is also responsible for the thickening of Tibetan crust and afterward extrusion of the Tibetan lithosphere
25   towards east.

Various models have been developed regarding the deformation of Tibet (Royden et al., 1997; Molnar and Tapponnier, 1975; Houseman and England, 1986, 1993, 1996; Tapponnier et al., 1982, 2001; Shen et al., 2001; Holt et al., 1995, 2000; Replumaz and Tapponnier, 2003; Flesch et al., 2001) but no single model can explain the whole scenario. The debate is open for understanding the deformation mechanism, crust and mantle deformation patterns and ongoing geodynamics. Multistage
30   subduction of Tethys oceanic plate and Indian plate below the Eurasian plate resulting in highly heterogeneous and anisotropic lithosphere is also discussed in recent works (Jagoutz et al., 2015; Van Hinsbergen et al., 2012). The Tibetan and Himalayan region is mainly dominated by thrust and strike slip faulting (Figure 1). Suture zones are extended in the E-W direction and take a sharp turn around eastern Himalayan Syntaxis (EHS). Strike slip faulting become more dominant to east of the EHS.

Figure 1 signifies that the eastern portion of the subducting Indian plate are found up to the EHS (León Soto et al., 2012) where the structural and topographical features takes a sharp trend in N-S striking from nearly E-W striking.

3 Data and Method

In this study we used a total of 5285 waveforms with the direct-S waves extracted from 161 teleseismic events with magnitudes ≥5.5 within an epicentral distance range from 30° to 90° (Figure 2). These teleseismic earthquakes used in this study are recorded at 47 seismic stations of the XE network, which was operated in between 2003-2004 (Sol et al., 2007) (Figure 3). Out of 47 stations we used only those 36 seismic stations where we have knowledge of seismic anisotropy (SKS splitting parameters measured by Sol et al. (2007) to be used when correcting for receiver-side anisotropy beneath the reference stations. Prior to the data analysis, we removed the instrument response from the original seismograms. At the stage of the preprocessing, a band-pass filter between 0.03 and 0.2 Hz was performed to enhance S signals and resampled the seismograms at 20 samples per seconds. Signals with any possible contaminations with other phases such as ScS, SKKS, and SKS are omitted from the analysis. We selected only those waveforms with a good signal to noise ratio (SNR) on transverse and radial components for further analysis. Waveform selection was achieved by performing a visual inspection manually that allowed only 40% of the direct-S waveforms. All the selected good quality waveforms show the characteristic of the splitting with clear energy on the transverse component and elliptically polarized particle motion. We started data analysis by determining station pairs over the entire area. Out of 355649 station pairs from 161 teleseismic events, we were left with 22816 station pairs within the interstation spacing of 300 km. We can use the Reference Station Technique (Eken and Tilmann, 2014) at a station pair only when four horizontal components of the same event are available at reference and target station. To minimize the effects of the coda waves and converted phases, we used a 45s time window starting 15s before the theoretical onset of the direct-S waves on the basis of the IASP91 1-D radial earth velocity model of Kennett (1991).

The approach used in the present study avoids the source side anisotropy by minimizing the misfit function between the corrected seismic waveforms at the reference and target stations. At the first stage an inverse splitting operator that consists of a backward angular rotation with two horizontal components and a time shift and the reversal of the backward rotation is employed to correct the reference station for known receiver-side anisotropy (generally inferred from SKS splitting analyses) when estimating of direct S-derived individual splitting parameters. Following the correction of the reference station S-signals at the target stations were corrected for arbitrary splitting parameters (ϕ and δt) in a grid search manner. Corrected S-wave signals at reference and target stations are compared to each other for each pair of arbitrary splitting parameters. Such comparison also allows for arbitrary time shifts and amplitude corrections to account for the lateral heterogeneities and differences in site response between these stations by optimizing the time shift ($\triangle$t) and amplitude factor (a). In the end, we selected final splitting parameters (FPD and TD) beneath the target station by minimizing the misfit function that simply represents the difference between corrected reference and target station traces.

The Reference Station Technique relies on two most important underlying assumptions: i) the distance between receiver and target stations is small compared to epicentral distance by virtue of that the ray path at these two stations can be considered

equivalent in deeper mantle part and near the source-side region, ii) waveform differences between the receiver and target stations are only due to difference in anisotropic structure after correcting any waveform differences in time and amplitude presumably due to the lateral heterogeneities and differences in site response between these stations. Any potential difference between the thickness of the crust and sedimentary layers will also cause the timing and amplitude of converted phase but

5   Eken and Tilmann (2014) earlier showed numerically its influence on expected splitting parameters would be negligible. The optimum interstation distance less than 300 km was previously validated for regional arrays by several application of the technique (e.g., Eken and Tilmann, 2014; Singh et al., 2016). During the application of the technique we let ϕ and δt to vary from 0 to 180° with an increment of 1° and 0 to 3 s with an increment of 0.05 s, respectively. We performed the inverse F-test error analysis of Silver and Chan (1991) for uncertainty estimates of obtained splitting parameters. In this process,

10   we checked reliability of the individual splitting parameter by comparing variation in the residual energy distribution away from the minimum with the variation according to preset confidence level. An example of the basic steps of the Reference Station Technique can be found in Figure 4 for target stations ES01 and ES03 respectively. Figure 5 presents the examples of the obtained splitting parameters with null at target stations ES19 and ES33, where we get null measurements by Sol et al. (2007). Null splitting may arise due to the two reasons: i) if the incoming polarization direction below an anisotropic

15   layer becomes parallel to the fast or slow axis; ii) if the region is isotropic in nature, due to complex anisotropy (e.g., Saltzer et al., 2000; Wüstefeld and Bokelmann, 2007). Following Eken and Tilmann (2014) and Singh et al. (2016) we also benefited from the F-test with the null-split rejection criteria to be able to avoid the contamination of the null measurement for the good splitting measurements. In this process, we theoretically calculate the residual energy under the assumption of the null measurements and compare this with the observed residual energy at the minimum. Figure 6 shows two examples of the null

20   splitting measurements at target stations ES29 and ES37 respectively. To ensure the stability of the results we have performed a stepwise quality assessment criterion before calculating the average splitting parameters at each station. To achieve this aim we considered only those waveform pairs that have (i) normalized residual energy ($\triangle$E) smaller than 0.5; (ii) amplitude correction factor parameter (a) in between 0.4 and 0.6; and (iii) $\geq 95\%$ confidence level for null splitting rejection. We rejected the waveform pairs that have an FPD error greater than 25° and delay time error greater than half of the delay time itself. After

25   these quality assessments we were left with only 3231 waveform pairs. At this stage of the processing we again performed another visual inspection manually to enhance the quality our estimates that finally allowed only 501 waveform pairs. These waveform pairs were extracted from only 25 teleseismic events and used to calculate the average splitting parameter at each station. We apply the Von Mises approach (Cochran et al., 2003) to calculate the circular mean at each target stations for ϕ and an arithmetic mean is used for δt.

30   **3.1   RESULTS**

We present here 501 splitting measurements observed for 42 seismic stations of the XE network between the years 2003 and 2004. Angular average of individual direct S-derived splitting parameters (ϕ_s and δt_s) at each station is given in Table 1. Station-averaged splitting parameters usually reflect that the significant anisotropy is present in the region. We observe a large variation in delay times ranging from 0.64 s to 1.68 s. By using the reference station technique, we revealed significant anisotropy in

areas where negligible anisotropy was reported earlier depending on only the SKS wave splitting measurements. For example at station ES31 direct-S waves provided relatively large time delay (1.23 s) although SKS splitting analysis performed by Sol et al. (2007) earlier resulted in a much smaller time delay about 0.3 s. In general, we observe the NE-SW to E-W trend in ϕ_s before the edge margin of the southeastern Tibetan region. A consistent change in variation of ϕ_s is observed further

5   east when orientations take a sharp change from ENE-SSW or E-W to NW-SE direction (Figure 7). We find the significant anisotropy ($\geq$0.64 s) at seismic stations ES19, ES20, ES22, ES32, ES33, ES34, ES42 and ES45, where previously hitherto null or negligible anisotropy were obtained with splitting of the SKS waves (Sol et al., 2007). This could stem from multi-layered anisotropic orientations or insufficient amount of SKS-derived splitting measurements. This rule out the consideration of the isotropic nature of the Indian lithosphere and signifies the complex 3D nature of more complex deformation pattern of the EHS.

10   The scatter plot in Figure 8 exhibits a comparison between estimated splitting parameters (ϕ_s and δt_s) from the analysis of direct-S wave and previous SKS splitting measurements (Sol et al., 2007). The overall trend of the obtained splitting parameters (ϕ_s) is consistent with the previous SKS measurement except at some places while generally observe the larger delay time of the S wave as compared to SKS wave.

    We combined our splitting study with the existing geodetic measurements (GPS velocity vector, APM velocity vector). We

15   plot the GPS velocities by using published data of Chen et al. (2000); Zhang et al. (2004); Shen et al. (2005); Sol et al. (2007). The APM velocities were calculated via a web-based plate motion calculator (https://www.unavco.org/software/geodetic-utilities/plate-motion-calculator/plate-motion-calculator.html) that is based on an integrated global plate motion model (GSRM v1.2) originally developed by Kreemer et al. (2003). Figure 9 simply presents a complex map, which reflects the correlative analysis of splitting parameters by using direct S-phases, APM directions, and GPS measurements in our targeted region. The

20   observation suggests that the observed anisotropy is not only due to lithospheric deformation or due to asthenospheric dynamics at the base of the lithosphere, but it is a combined effect of both

3.2   DISCUSSION

3.3   Origin of anisotropy in the Southeastern Tibetan region

Our resultant splitting measurements varying in a range of δt_s from 0.64 to 1.68 s suggest presence of very complex deformation

25   types in the region. The fast polarization directions are rather consistent and matching well with the surface geology similar to those observed from the SKS phases in Sol et al. (2007). The fast axis closely follow the follow the strike of the major sutures like BNSZ and ITSZ and surface strain fields as observed through GPS and are under the influence of bending at Eastern Himalayan Syntaxis (Figure 7). Vertically coherent deformation of the crust and upper mantle are associated to the seismic anisotropy directions parallel to the surface geologic features such as faults etc. (e.g., Savage, 1999; Flesch et al., 2005) and

30   earlier has been invoked as a possibility to explain the anisotropic character in the eastern and northeastern Tibet (Holt et al., 2000; León Soto et al., 2012; Eken et al., 2013; Eken and Tilmann, 2014). Mechanically coupled crust-mantle interface or coherent deformation of whole lithosphere with similar boundary conditions are used to exaplin the observed anisotropy in eastern Tibet (Holt et al., 2000; Sol et al., 2007). In absence of any compelling evidence for crust-mantle coupling, we argued

in favor of a large scale deformation of crust and upper mantle under similar boundary conditions as plausible option to explain the observed anisotropy (Flesch et al., 2005; Sol et al., 2007; Holt et al., 2000).

Observed larger time delays (>1s), in this study, reflect a highly anisotropic region with similar deformation patterns at depths. Presence of a more complex anisotropic structure (e.g. double-layer) with different orientation in fast axis at various depths may result in smaller delay times (Saltzer et al., 2000). In the western Himalayan region, Vinnik et al. (2007) observed the different orientation of the fast direction of seismic azimuthal anisotropy from 60° at 80-160 km to 150° at 160-220 km depth region by using the joint inversion of the SKS particle motion and P receiver functions. This provides an argument to explain the null or negligible anisotropy as reported from the same region using SKS phases (Sandvol et al., 1994). Smaller time delays in Nepal Himalaya and Sikkim Himalaya were attributed to the combined effect of shear at the base of lithosphere due to APM related strain of Indian plate and ductile flow along the collision front due to compression, with possibly completely different orientations (Singh et al., 2007). Null measurements were reported at few stations used in the present study by Sol et al. (2007) using SKS/SKKS phases, although no specific reasons are provided. The transition between deformation types at the boundaries of Indian and Eurasian lithospheric plates was considered to be the main reason for observed null or negligible anisotropy further west beneath southern Tibetan Plateau (Chen et al., 2010; Chen and Ozalaybey, 1998; Barruol and Hoffmann, 1999; Zhao et al., 2014). The lack of anisotropy beneath southern Tibet was mainly explained by the isotropic nature of Indian tectonic plate or lack in ability of SKS phases to sample the anisotropy due to sub-vertical mantle shear strain field created due to downwelling Indian lithosphere (Singh et al., 2007; Sandvol et al., 1997). However the isotropic nature of Indian lithosphere was contradicted in various studies (Singh et al., 2006, 2007; Kumar and Singh, 2008) and significant anisotropy is reported beneath Tibet in region of null (Gao and Liu, 2009; Singh et al., 2016). Indian lithosphere is considered to be more isotropic in nature to explain the null or negligible anisotropy beneath southern Tibet (Chen and Ozalaybey, 1998; Barruol and Hoffmann, 1999; Chen et al., 2010). Taking forward the same argument to explain the null measurements at few specific stations beneath Namchebarwa Mountains requires the northern extent of the Indian lithospheric mantle north of ITSZ. The recent tomographic studies (Griot et al., 1998; Huang et al., 2003; Zhou and Murphy, 2005; Yao et al., 2008; Priestley et al., 2006; Singh et al., 2014; Pandey et al., 2014) suggest that in the western Tibetan side where the N-S extension is less, the Indian lithosphere is supposed to be up to the Jinsa River Suture Zone (JRSZ) (Zhao et al., 2010), while in the eastern Tibet side the Indian lithosphere is extending up to the ITCZ (Li et al., 2008; Zhao et al., 2010). Combined study using seismic anisotropy and Bouguer gravity anomalies placed the Indian mantle front up to 33° N in central Tibet (Chen et al., 2010). In the present segment of the Himalaya-Tibet collision zone northern limit of the Indian lithospheric mantle does not seem to extend beyond ITSZ (Li et al., 2008). The lack of anisotropy reported using SKS/SKKS phases (Sol et al., 2007) at few seismic stations may be due to insufficient measurements. By adding considerably large amount of measurements from direct-S waves we observe significant anisotropy for the same stations and fast axis deformation can be explained by eastward flow in a lithospheric crush zone as suggested for southern Tibet (Zhao et al., 2014).

The crust beneath Tibet is thick (~ 80 km, Singh et al. (2015)) and crustal anisotropic effects should be accounted in the splitting measurements obtained using direct-S and SKS/SKKS phases. In the Himalayan region highly anisotropic crust (~20%) has been reported using inversion of receiver functions (Schulte-Pelkum et al., 2005; Singh et al., 2010), while similar

approach at few seismic stations covering Tibet suggests for 4-14% seismic anisotropy within the Tibetan crust (Sherrington et al., 2004; Ozacar and Zandt, 2004). Ozacar and Zandt (2004) have accounted for splitting of <0.5 s over SKS split times due to the observed anisotropy of > 10% in the crust. Splitting time of 0.2-0.3 s is observed within the eastern Tibet crust using splitting of Moho converted Ps phases (receiver functions) (Chen et al., 2013). Tomographic (Huang et al., 2002, 2009; Hung

5 et al., 2010; Yao et al., 2008, 2010; Li et al., 2009), magnetotelluric (Bai et al., 2010) and gravity (Jordan and Watts, 2005) studies of the SE Tibetan region suggest for a ductile flow of the deeper region in the crust. The variation pattern of the shear wave in the tomographic studies at these crustal depths suggest the localized flow of the crustal material along strike slip fault network in the region (Yao et al., 2010). These types of flow may produce splitting orientations similar to lower lithospheric scales with coherent deformation. Considering a coupled crust and mantle with coherent deformation may increase the SKS

10 delay times by 0.2-0.5 s due to the effects of crust. The anisotropic orientations observed beneath most parts of the Tibet (Sherrington et al., 2004; Ozacar and Zandt, 2004; Chen et al., 2013) within the crust are completely different than the SKS or direct-S waves implying the types pf deformation in the crust and upper mantle could be completely different and does not indicate a coherent deformation at least in parts of Tibet. The most possible explanation for such decoupling could be that the crustal anisotropic parameters are influenced by either current deformation or fossilized fabric with different boundary

15 conditions at mid-crustal and lower crustal levels .

3.4 Comparison between direct S and SKS derived splitting parameters

The scatter plot in Figure 8 exhibits a comparison between estimated splitting parameters (ϕ_s and δt_s) from the analysis of direct-S wave and previous SKS splitting measurements (Sol et al., 2007). The obtained splitting parameters (ϕ_s) from the direct-S wave measurements depict that it is consistent with the previous SKS measurements except at some places. Overall

20 consistency between splitting parameters inferred from SKS and direct-S waves is most likely due to the fact that both are exposed to the same sort of large-scale anisotropic structures. Large differences between SKS- and S-derived δt_s that appear as a move-out in the scatter plot is occur due to the two reason: i) longer travelling paths of the direct-S waves as compared to the SKS exposed for the same type of the of large scale anisotropy and, ii) large number of the events from different azimuths contributing to the direct-S wave measurements as compared to the SKS. The accuracy of the measurements relies on more

25 measurements and direct-S waves splitting measurements supplement the splitting measurements from the region. Comparative studies of the splitting parameters obtained from the direct-S waves are in close agreement to the SKS splitting measurements as observed in the Himalaya- Tibet collision zone (e.g., McNamara et al., 1994; Singh et al., 2016; Huang et al., 2011; Eken et al., 2013) and in the Indian shield (Saikia et al., 2010)

3.5 Deformation pattern revealed from the comparison of the GPS, APM and splitting measurements

30 Previous studies on seismic anisotropy (McNamara et al., 1994; Sol et al., 2007; Huang et al., 2000, 2007; Wang et al., 2007, 2008; Chen et al., 2013; Zhao et al., 2014; Guilbert et al., 1996; Bai et al., 2009) that compared splitting parameters with those of APM, GPS and structural and topographical features provided crucial information about to understand the dynamic deformation pattern and possible linkage of the strength of the coupling in between the crust and lithospheric mantle of the

southeastern or eastern Tibetan region. We observe a sharp transition in the spatial distribution of ϕ_s due to change in the fast polarization direction from the nearly east west direction to nearly NE to SW or NNE to SSW near the edge margin of the southeastern Tibet. Structural and topographical feature such as major suture zones, mountain belts, etc. tends to rotate around the EHS from nearly E-W or ENE-WSW to N-S or NE-SW direction (Hallet and Molnar, 2001; Booth et al., 2004).

5 The observed FPDs and GPS velocity vectors follow nearly the similar trend. The absolute plate motion (APM) directions are well consistent with the present ongoing asthenospheric flow (Vinnik et al., 1992, 1995; Vinnik and Montagner, 1996). The FPDs overall do not match with the APM velocity direction of Indian plate with respect to Eurasian plate or with the APM velocity of the Eurasian plate and Indian plate with respect to fixed frame or no-net rotation frame. The discrepancy between the FPD and APM may indicate that the obtained splitting and hence the anisotropic behavior of the study area is not only

10 due to asthenospheric dynamics but it is a combined effect of the lithospheric deformation and asthenospheric dynamics. The lateral variation of obtained splitting measurements, when taken together with GPS velocity vectors, geological features and the APM directions depict the movement of lithospheric or crustal material of western and central plateau relative to Eurasian plate towards the eastern Tibetan side and clockwise rotation around the EHS. This support the idea of deep crustal flow and the movement of material from the central and western portion towards the eastern Tibetan side that have been earlier suggested

15 by Royden et al. (1997, 2008).

The present day GPS measurement does not reveal the deformation of the whole crust but could be rather associated to the deformation of the shallow crust (Chen et al., 2013). Results from earlier receiver functions-based imaging studies on crustal anisotropy (see Sherrington et al. (2004); Chen et al. (2013)) were in a way to support this argument. The orientation of the GPS velocity and the FPDs of the direct-S waves exactly match only when the orientation of the different layers of the anisotropy

20 within the crust and mantle follow the similar orientation. Griot et al. (1998); Holt et al. (2000); Fouch et al. (2000); Sol et al. (2007) discuss about the coupling and decoupling of the crust and mantle by making comparisons among the FPD, GPS, APM and surficial features. According to Sol et al. (2007)Sol et al. (2007) coupling between the crustal and mantle material for the entire southeastern Tibetan region existed as similarly observed in the northeast Tibetan plateau (e.g., Eken et al., 2013; Eken and Tilmann, 2014). The seismic anisotropy directions that were previously obtained from the inversion of receiver functions,

25 however, do not suggest vertically coherent deformation of the crust (e.g., Ozacar and Zandt, 2004; Sherrington et al., 2004). One possibility for this mismatch could be due to the nature of receiver functions analyses that are prone to be sensitive to rather fossilized fabrics representing complex deformation history of the crust in Tibet although crust is deformed coherently.

On the basis of driving forces, two kinematic models have been proposed to explain the coupling- decoupling of the crust and lithospheric mantle. First one is simple asthenospheric model (Richardson, 1992) proposed to explain the decoupling of

30 the crust and mantle by intruding the weak mechanical layer such as asthenosphere and other in the crust. Whenever a weak mechanical layer is present in between the crust and mantle the force acted on the crustal region cannot be transmitted into the mantle. As a result crust is decoupled from the mantle due to different driving forces acted on them. In such model velocity difference between the top and bottom of the weak mechanical layer give rise to the mantle deformation and that difference is parallel to the fast polarization direction. Second model proposed by Lithgow-Bertelloni and Richards (1998) is the vertical

35 coherent model and it explains the coupling of the materials within the crust and lithospheric mantle on the basis of transmission

of the buoyancy forces from crust to the mantle. This model requires a rigid lower part of the crust. However recent the low shear wave velocity anomalies resolved in various tomographic studies recently (Huang et al., 2002, 2009; Hung et al., 2010; Yao et al., 2008; Li et al., 2009) have indicated a weak layer in the deeper region of the crust beneath the SE Tibetan region by contradicts this. It is noteworthy to mention that we avoid making any comment on the possible linkage between deformation

5   and coupling of crust and underlying lithospheric mantle by only using splitting parameters inferred from direct-S waves and geodetic measurements.

4   Conclusions

Our splitting observations using direct-S waves add new constraints in understanding the deformation pattern and their causes in the southeastern Tibetan region near Namche Barwa. We can list main concluding remarks from the present study as follows:

10   1. The observed splitting analysis suggests for a highly deformed crust and lithospheric mantle.

2. Significant anisotropy at stations where null or negligible anisotropy is reported using SKS measurements, rules out the hypothesis of the isotropic lithospheric mantle.

3. Our study also provided clear evidences for the development of anisotropy in this region with strong geodynamic implications of several tectonic events, i.e., the multistage subduction of Indian plate below the Eurasian plate, the movement of the

15   western central Tibetan lithospheric material towards the southeastern and eastern Tibetan side and rollback towards Burma.

4. The observed anisotropy delays (0.67-1.68) suggest for possible existence of a multi-layered anisotropy structure in the crust and upper mantle. Further understanding this requires 3-D geodynamic modeling and inversion of multi-frequency datasets to resolve more complex depth-dependent anisotropic structures (e.g. multi-layer anisotropy, dipping axis of symmetry).

20   ## 5   Code availability

The multisplit C++ code used for carrying out splitting measurements of the direct S waveforms is available with a General Public License (GPL) license at http://github.com/ftilmann/multisplit.

6   Data availability

The waveform data used in this study are downloaded from the Incorporated Research Institutions for Seismology Data Man-

25   agement Center (IRIS-DMC) data archive system Namche Barwa Tibet network code XE (2003-2004).

Acknowledgements. The IRIS data management centre and Project team of Nameche Barwa Seismic network (PASSCAL) are gratefully acknowledged for making the seismic data available. This work has been performed under the ISIRD project (ASI) of IIT Kharagpur. T. Eken appreciates the Alexander-von-Humboldt (AvH) foundation for the postdoctoral scholarship as well as equipment subsidy that have contributed greatly at different stages of the development of the main software (multisplit) used in the present study.

References

Ando, M.: ScS polarization anisotropy around the Pacific Ocean., Journal of Physics of the Earth, 32, 179–195, doi:10.4294/jpe1952.32.179, 1984.

Argand, E.: La tectonique de l'Asie, Int. geol, Congr. Rep, pp. 171–322, 1924.

5 Bai, D., Unsworth, M. J., Meju, M. A., Ma, X., Teng, J., Kong, X., Sun, Y., Sun, J., Wang, L., Jiang, C., et al.: Crustal deformation of the eastern Tibetan plateau revealed by magnetotelluric imaging, Nature geoscience, 3, 358–362, doi:10.1038/ngeo830, 2010.

Bai, L., Iidaka, T., Kawakatsu, H., Morita, Y., and Dzung, N.: Seismic anisotropy and shear-wave splitting in lower-crustal and upper-mantle rocks from the Ivrea Zone—experimental and calculated data, Phys. Earth Planet. Inter., 176, 33–43, doi:10.1016/j.pepi.2009.03.008, 2009.

10 Barruol, G. and Hoffmann, R.: Upper mantle anisotropy beneath the Geoscope stations, J. Geophys. Res., 104, 10 757–10 773, doi:10.1029/1999JB900033, 1999.

Becker, T. W. and Faccenna, C.: Mantle conveyor beneath the Tethyan collisional belt, Earth Planet. Sci. Lett., 310, 453 – 461, doi:10.1016/j.epsl.2011.08.021, 2011.

Booth, A. L., Zeitler, P. K., Kidd, W. S., Wooden, J., Liu, Y., Idleman, B., Hren, M., and Chamberlain, C. P.: U-Pb zircon constraints on the tectonic evolution of southeastern Tibet, Namche Barwa Area, American Journal of Science, 304, 889–929, doi:10.2475/ajs.304.10.889, 2004.

Bormann, P., Grünthal, G., Kind, R., and Montag, H.: Upper mantle anisotropy beneath central Europe from SKS wave splitting: effects of absolute plate motion and lithosphere-asthenosphere boundary topography?, J. Geodynamics, 22, 11–32, doi:10.1016/0264-3707(96)00014-2, 1996.

20 Chen, W.-P. and Ozalaybey, S.: Correlation between seismic anisotropy and Bouguer gravity anomalies in Tibet and its implications for lithospheric structures, Geophys. J. Int., 135, 93–101, doi:10.1046/j.1365-246X.1998.00611.x, 1998.

Chen, W.-P., Martin, M., Tseng, T.-L., Nowack, R. L., Hung, S.-H., and Huang, B.-S.: Shear-wave birefringence and current configuration of converging lithosphere under Tibet, Earth Planet. Sci. Lett., 295, 297 – 304, doi:10.1016/j.epsl.2010.04.017, 2010.

Chen, Y., Zhang, Z., Sun, C., and Badal, J.: Crustal anisotropy from Moho converted Ps wave splitting analysis and geodynamic implications beneath the eastern margin of Tibet and surrounding regions, Geophys. Res. Lett., 24, 946–957, doi:10.1016/j.gr.2012.04.003, 2013.

Chen, Z., Burchfiel, B., Liu, Y., King, R., Royden, L., Tang, W., Wang, E., Zhao, J., and Zhang, X.: Global Positioning System measurements from eastern Tibet and their implications for India/Eurasia intercontinental deformation, J. Geophys. Res., 105, 16 215–16 227, doi:10.1029/2000JB900092, 2000.

Christensen, N. I.: Elasticity of Ultrabasic Rocks, J. Geophys. Res., 71, 5921–5931, doi:10.1029/JZ071i024p05921, 1966.

30 Cochran, E. S., Vidale, J. E., and Li, Y.-G.: Near-fault anisotropy following the Hector Mine earthquake, JGR, 108, n/a–n/a, doi:10.1029/2002JB002352, 2003.

Eken, T. and Tilmann, F.: The Use of Direct Shear Waves in Quantifying Seismic Anisotropy: Exploiting Regional Arrays, Bull. Seismol. Soc. Am., 104, 2644–2661, doi:10.1785/0120140020, 2014.

Eken, T., Tilmann, F., Mechie, J., Zhao, W., Kind, R., Su, H., Xue, G., and Karplus, M.: Seismic Anisotropy from SKS Splitting beneath Northeastern Tibet, Bull. Seismol. Soc. Am., 103, 3362–3371, doi:10.1785/0120130054, 2013.

35

Flesch, L. M., Haines, A. J., and Holt, W. E.: Dynamics of the India-Eurasia collision zone, J. Geophys. Res., 106, 16 435–16 460, doi:10.1029/2001JB000208, 2001.

Flesch, L. M., Holt, W. E., Silver, P. G., Stephenson, M., Wang, C.-Y., and Chan, W. W.: Constraining the extent of crust–mantle coupling in central Asia using GPS, geologic, and shear wave splitting data, Earth Planet. Sci. Lett., 238, 248 – 268, doi:10.1016/j.epsl.2005.06.023, 2005.

Fouch, M. J. and Rondenay, S.: Seismic anisotropy beneath stable continental interiors, Phys. Earth Planet. Inter., 158, 292 – 320, doi:10.1016/j.pepi.2006.03.024, continental Anisotropy, 2006.

Fouch, M. J., Fischer, K. M., Parmentier, E. M., Wysession, M. E., and J., C. T.: Shear wave splitting, continental keels, and patterns of mantle flow, J. Geophys. Res., 105, 6255–6275, doi:10.1029/1999JB900372, 2000.

Fu, Y. V., Chen, Y. J., Li, A., Zhou, S., Liang, X., Ye, G., Jin, G., Jiang, M., and Ning, J.: Indian mantle corner flow at southern Tibet revealed by shear wave splitting measurements, Geophys. Res. Lett., 35, n/a–n/a, doi:10.1029/2007GL031753, 2008.

Fukao, Y.: Evidence from core-reflected shear waves for anisotropy in the Earth's mantle, Nature, 309, 695–698, doi:10.1038/309695a0, 1984.

Gao, S. S. and Liu, K. H.: Significant seismic anisotropy beneath the southern Lhasa Terrane, Tibetan Plateau, Geochem., Geophys., Geosys., 10, n/a–n/a, doi:10.1029/2008GC002227, 2009.

Garzanti, E. and Van Haver, T.: The Indus clastics: forearc basin sedimentation in the Ladakh Himalaya (India), SG, 59, 237–249, doi:10.1016/0037-0738(88)90078-4, 1988.

Griot, D.-A., Montagner, J.-P., and Tapponnier, P.: Phase velocity structure from Rayleigh and Love waves in Tibet and its neighboring regions, J. Geophys. Res., 103, 21 215–21 232, doi:10.1029/98JB00953, 1998.

Guilbert, J., Poupinet, G., and Mei, J.: A study of azimuthal P residuals and shear-wave splitting across the Kunlun range (Northern Tibetan plateau), Phys. Earth Planet. Inter., 95, 167–174, doi:10.1016/0031-9201(95)03120-0, 1996.

Hallet, B. and Molnar, P.: Distorted drainage basins as markers of crustal strain east of the Himalaya, J. Geophys. Res., 106, 13 697–13 709, doi:10.1029/2000JB900335, 2001.

Henderson, A. L., Najman, Y., Parrish, R., Mark, D. F., and Foster, G. L.: Constraints to the timing of India–Eurasia collision; a re-evaluation of evidence from the Indus Basin sedimentary rocks of the Indus–Tsangpo Suture Zone, Ladakh, India, Earth-Sci. Rev., 106, 265–292, doi:10.1016/j.earscirev.2011.02.006, 2011.

Herquel, G., Wittlinger, G., and Guilbert, J.: Anisotropy and crustal thickness of northern-Tibet. New constraints for tectonic modelling, Geophys. Res. Lett., 22, 1925–1928, doi:10.1029/95GL01789, 1995.

Hirn, A., Jiang, M., Sapin, M., Diaz, J., Nercessian, A., and Lu, Q.: Seismic anisotropy as an indicator of mantle flow beneath the Himalayas and Tibet, Nature, 375, 571–574, doi:10.1038/375571a0, 1995.

Holt, W., Chamot-Rooke, N., Le Pichon, X., Haines, A., Shen-Tu, B., and Ren, J.: Velocity field in Asia inferred from Quaternary fault slip rates and Global Positioning System observations, J. Geophys. Res., 105, 19 185–19 209, doi:10.1029/2000JB900045, 2000.

Holt, W. E., Li, M., and Haines, A.: Earthquake strain rates and instantaneous relative motions within central and eastern Asia, Geophys. J. Int., 122, 569–593, doi:10.1111/j.1365-246X.1995.tb07014.x, 1995.

Houseman, G. and England, P.: Finite strain calculations of continental deformation: 1. Method and general results for convergent zones, J. Geophys. Res., 91, 3651–3663, doi:10.1029/JB091iB03p03651, 1986.

Houseman, G. and England, P.: Crustal thickening versus lateral expulsion in the Indian-Asian continental collision, J. Geophys. Res., 98, 12 233–12 249, doi:10.1029/93JB00443, 1993.

Houseman, G. and England, P.: A lithospheric-thickening model for the Indo-Asian collision, WORLD AND REGIONAL GEOLOGY, 1, 1–17, 1996.

Huang, J., Zhao, D., and Zheng, S.: Lithospheric structure and its relationship to seismic and volcanic activity in southwest China, J. Geophys. Res., 107, ESE 13–1–ESE 13–14, doi:10.1029/2000JB000137, 2002.

Huang, W.-C., Ni, J. F., Tilmann, F., Nelson, D., Guo, J., Zhao, W., Mechie, J., Kind, R., Saul, J., Rapine, R., and Hearn, T. M.: Seismic polarization anisotropy beneath the central Tibetan Plateau, J. Geophys. Res., 105, 27 979–27 989, doi:10.1029/2000JB900339, 2000.

5 Huang, Z., Wang, L., Xu, M., Liu, J., Mi, N., and Liu, S.: Shear wave splitting across the Ailao Shan-Red River fault zone, SW China, Geophys. Res. Lett., 34, n/a–n/a, doi:10.1029/2007GL031236, 2007.

Huang, Z., Li, H., Zheng, Y., and Peng, Y.: The lithosphere of North China Craton from surface wave tomography, Earth Planet. Sci. Lett., 288, 164–173, doi:10.1016/j.epsl.2009.09.019, 2009.

Huang, Z., Wang, L., Zhao, D., Mi, N., and Xu, M.: Seismic anisotropy and mantle dynamics beneath China, Earth Planet. Sci. Lett., 306, 10 105 – 117, doi:10.1016/j.epsl.2011.03.038, 2011.

Huang, Z.-M., Zhang, Y.-Z., Kotaki, M., and Ramakrishna, S.: A review on polymer nanofibers by electrospinning and their applications in nanocomposites, Composites science and technology, 63, 2223–2253, doi:10.1016/S0266-3538(03)00178-7, 2003.

Hung, S.-H., Chen, W.-P., Chiao, L.-Y., and Tseng, T.-L.: First multi-scale, finite-frequency tomography illuminates 3-D anatomy of the Tibetan plateau, Geophys. Res. Lett., 37, n/a–n/a, doi:10.1029/2009GL041875, 2010.

15 Jagoutz, O., Royden, L., Holt, A. F., and Becker, T. W.: Anomalously fast convergence of India and Eurasia caused by double subduction, Nature Geoscience, 8, 475–478, doi:10.1038/ngeo2418, 2015.

Jordan, T. and Watts, A.: Gravity anomalies, flexure and the elastic thickness structure of the India–Eurasia collisional system, Earth Planet. Sci. Lett., 236, 732–750, doi:10.1016/j.epsl.2005.05.036, 2005.

Kaneshima, S. and Silver, P. G.: Anisotropic loci in the mantle beneath central Peru, Phys. Earth Planet. Inter., 88, 257 – 272, 20 doi:10.1016/0031-9201(94)02981-G, 1995.

Karato, S.-I.: Grain-size distribution and rheology of the upper mantle, Tectonophys, 104, 155–176, doi:1016/0040-1951(84)90108-2, 1984.

Karato, S.-I.: Seismic anisotropy due to lattice preferred orientation of minerals: Kinematic or dynamic?, Geophysical Monograph Series., 39, 455–471, doi:10.1029/GM039p0455, 1987.

Karato, S.-i. and Wu, P.: Rheology of the Upper Mantle: A Synthesis, Science, 260, 771–778, doi:10.1126/science.260.5109.771, 1993.

25 Karplus, M., Zhao, W., Klemperer, S., Wu, Z., Mechie, J., Shi, D., Brown, L., and Chen, C.: Injection of Tibetan crust beneath the south Qaidam Basin: Evidence from INDEPTH IV wide-angle seismic data, J. Geophys. Res., 116, n/a–n/a, doi:10.1029/2010JB007911, 2011.

Keith, C. M. and Crampin, S.: Seismic body waves in anisotropic media: Propagation through a layer, Geophys. J. Int., 49, 209–223, doi:10.1111/j.1365-246X.1977.tb03709.x, 1977.

Kennett, B. L. N.and Engdahl, E.: Traveltimes for global earthquake location and phase identification, Geophys. J. Int., 105, 429–465, 30 doi:10.1111/j.1365-246X.1991.tb06724.x, 1991.

Kind, R., Kosarev, G., Makeyeva, L., and Vinnik, L.: Observations of laterally inhomogeneous anisotropy in the continental lithosphere, Nature, 318, 358–361, doi:10.1038/318358a0, 1985.

Kreemer, C., Holt, W. E., and Haines, A. J.: An integrated global model of present-day plate motions and plate boundary deformation, Geophys. J. Int., 154, 8–34, doi:10.1046/j.1365-246X.2003.01917.x, 2003.

35 Kumar, M. R. and Singh, A.: Evidence for plate motion related strain in the Indian shield from shear wave splitting measurements, J. Geophys. Res., 113, n/a–n/a, doi:10.1029/2007JB005128, 2008.

Kumar, P., Yuan, X., Kind, R., and Ni, J.: Imaging the colliding Indian and Asian lithospheric plates beneath Tibet, J. Geophys. Res., 111, n/a–n/a, doi:10.1029/2005JB003930, b06308, 2006.

Lavé, J., Avouac, J., Lacassin, R., Tapponnier, P., and Montagner, J.: Seismic anisotropy beneath Tibet: evidence for eastward extrusion of the Tibetan lithosphere?, EPSL, 140, 83–96, doi:10.1016/0012-821X(96)00045-3, 1996.

León Soto, G., Sandvol, E., Ni, J. F., Flesch, L., Hearn, T. M., Tilmann, F., Chen, J., and Brown, L. D.: Significant and vertically coherent seismic anisotropy beneath eastern Tibet, J. Geophys. Res., 117, n/a–n/a, doi:10.1029/2011JB008919, 2012.

5 Lev, E., Long, M. D., and van der Hilst, R. D.: Seismic anisotropy in Eastern Tibet from shear wave splitting reveals changes in lithospheric deformation, EPSL, 251, 293–304, doi:10.1016/j.epsl.2006.09.018, 2006.

Li, C., Van der Hilst, R. D., Meltzer, A. S., and Engdahl, E. R.: Subduction of the Indian lithosphere beneath the Tibetan Plateau and Burma, EPSL, 274, 157–168, doi:10.1016/j.epsl.2008.07.016, 2008.

Li, Y. H., Wu, Q. J., and Tian, X. B.: Crustal structure in the Yunnan region determined by modeling receiver functions, Chinese J. Geophys.,
10 52, 67–80, 2009.

Lithgow-Bertelloni, C. and Richards, M. A.: The dynamics of Cenozoic and Mesozoic plate motions, Rev. Geophys., 36, 27–78, doi:10.1029/97RG02282, 1998.

Mainprice, D., Barruol, G., and Ismail, W. B.: The seismic anisotropy of the Earth's mantle: from single crystal to polycrystal, Earth's Deep Interior: Mineral physics and tomography from the atomic to the global scale, pp. 237–264, doi:10.1029/GM117p0237, 2000.

15 McKenzie, D. and Priestley, K.: The influence of lithospheric thickness variations on continental evolution, Lithos, 102, 1–11, doi:10.1016/j.lithos.2007.05.005, 2008.

McNamara, D. E., Owens, T. J., Silver, P. G., and Wu, F. T.: Shear wave anisotropy beneath the Tibetan Plateau, J. Geophys. Res., 99, 13 655–13 665, doi:10.1029/93JB03406, 1994.

Molnar, P. and Tapponnier, P.: Cenozoic tectonics of Asia: effects of a continental collision, Science, 189, 419–426,
20 doi:10.1126/science.189.4201.419, 1975.

Nelson, K. D., Zhao, W., Brown, L., Kuo, J., Che, J., Liu, X., Klemperer, S., Makovsky, Y., Meissner, R., Mechie, J., et al.: Partially molten middle crust beneath southern Tibet: synthesis of project INDEPTH results, Science, 274, 1684–1688, doi:10.1126/science.274.5293.1684, 1996.

Nicolas, A. and Christensen, N. I.: Formation of Anisotropy in Upper Mantle Peridotites-A Review, Composition, structure and dynamics of
25 the lithosphere-asthenosphere system, pp. 111–123, doi:10.1029/GD016p0111, 1987.

Ozacar, A. A. and Zandt, G.: Crustal seismic anisotropy in central Tibet: Implications for deformational style and flow in the crust, Geophys. Res. Lett., 31, n/a–n/a, doi:10.1029/2004GL021096, 2004.

Pandey, S., Yuan, X., Debayle, E., Priestley, K., Kind, R., Tilmann, F., and Li, X.: A 3D shear-wave velocity model of the upper mantle beneath China and the surrounding areas, Tectonophys, 633, 193–210, doi:10.1016/j.tecto.2014.07.011, 2014.

30 Priestley, K., Debayle, E., McKenzie, D., and Pilidou, S.: Upper mantle structure of eastern Asia from multimode surface waveform tomography, J. Geophys. Res., 111, n/a–n/a, doi:10.1029/2005JB004082, 2006.

Replumaz, A. and Tapponnier, P.: Reconstruction of the deformed collision zone between India and Asia by backward motion of lithospheric blocks, J. Geophys. Res., 108, n/a–n/a, doi:10.1029/2001JB000661, 2003.

Richardson, R.: Ridge forces, absolute plate motions, and the intraplate stress field, J. Geophys. Res., 97, 11 739–11 748,
35 doi:10.1029/91JB00475, 1992.

Rowley, D. B. and Currie, B. S.: Palaeo-altimetry of the late Eocene to Miocene Lunpola basin, central Tibet, Nature, 439, 677–681, doi:10.1038/nature04506, 2006.

Royden, L. H., Burchfiel, B. C., King, R. W., Wang, E., Chen, Z., Shen, F., and Liu, Y.: Surface deformation and lower crustal flow in eastern Tibet, Science, 276, 788–790, doi:10.1126/science.276.5313.788, 1997.

Royden, L. H., Burchfiel, B. C., and van der Hilst, R. D.: The geological evolution of the Tibetan Plateau, Science, 321, 1054–1058, doi:10.1126/science.1155371, 2008.

5 Saikia, D., Ravi Kumar, M., Singh, A., Mohan, G., and Dattatrayam, R. S.: Seismic anisotropy beneath the Indian continent from splitting of direct S waves, J. Geophys. Res., 115, n/a–n/a, doi:10.1029/2009JB007009, 2010.

Saltzer, R. L., Gaherty, J. B., and Jordan, T. H.: How are vertical shear wave splitting measurements affected by variations in the orientation of azimuthal anisotropy with depth?, Geophys. J. Int., 141, 374–390, doi:10.1046/j.1365-246X.2000.00088.x, 2000.

Sandvol, E., Ni, J., Kind, R., and Zhao, W.: Seismic anisotropy beneath the southern Himalayas-Tibet collision zone, J. Geophys. Res., 102,
10   17 813–17 823, doi:10.1029/97JB01424, 1997.

Sandvol, E. A., Ni, J. F., Hearn, T. M., and Roecker, S.: Seismic azimuthal anisotropy beneath the Pakistan Himalayas, Geophys. Res. Lett., 21, 1635–1638, doi:10.1029/94GL01386, 1994.

Sato, H., Fehler, M. C., and Maeda, T.: Seismic wave propagation and scattering in the heterogeneous earth, vol. 496, Springer, doi:10.1007/978-3-540-89623-4, 2012.

15 Savage, M. K.: Seismic anisotropy and mantle deformation: What have we learned from shear wave splitting?, Rev. Geophys., 37, 65–106, doi:10.1029/98RG02075, 1999.

Schulte-Pelkum, V., Monsalve, G., Sheehan, A., Pandey, M. R., Sapkota, S., Bilham, R., and Wu, F.: Imaging the Indian subcontinent beneath the Himalaya, Nature, 435, 1222–1225, doi:10.1038/nature03678, 2005.

Shen, F., Royden, L. H., and Burchfiel, B. C.: Large-scale crustal deformation of the Tibetan Plateau, J. Geophys. Res., 106, 6793–6816,
20   doi:10.1029/2000JB900389, 2001.

Shen, Z.-K., Lü, J., Wang, M., and Bürgmann, R.: Contemporary crustal deformation around the southeast borderland of the Tibetan Plateau, J. Geophys. Res., 110, n/a–n/a, doi:10.1029/2004JB003421, 2005.

Sherrington, H. F., Zandt, G., and Frederiksen, A.: Crustal fabric in the Tibetan Plateau based on waveform inversions for seismic anisotropy parameters, JGR, 109, n/a–n/a, doi:10.1029/2002JB002345, 2004.

25 Silver, P. G. and Chan, W. W.: Implications for continental structure and evolution from seismic anisotropy, Nature, 335, 34–39, doi:10.1038/335034a0, 1988.

Silver, P. G. and Chan, W. W.: Shear wave splitting and subcontinental mantle deformation, JGR, 96, 16 429–16 454, doi:10.1029/91JB00899, 1991.

Singh, A., Kumar, M. R., Raju, P. S., and Ramesh, D. S.: Shear wave anisotropy of the northeast Indian lithosphere, Geophys. Res. Lett., 33,
30   doi:10.1029/2006GL026106, 2006.

Singh, A., Kumar, M. R., and Raju, P. S.: Mantle deformation in Sikkim and adjoining Himalaya: Evidences for a complex flow pattern, Phys. Earth Planet. Inter., 164, 232–241, doi:10.1016/0031-9201(93)90156-4, 2007.

Singh, A., Kumar, M. R., and Raju, P. S.: Seismic structure of the underthrusting Indian crust in Sikkim Himalaya, Tectonics, 29, doi:10.1029/2010TC002722, 2010.

35 Singh, A., Mercier, J.-P., Ravi Kumar, M., Srinagesh, D., and Chadha, R. K.: Continental scale body wave tomography of India: Evidence for attrition and preservation of lithospheric roots, Geochem., Geophys., Geosys., 15, 658–675, doi:10.1002/2013GC005056, 2014.

Singh, A., Singh, C., and Kennett, B.: A review of crust and upper mantle structure beneath the Indian subcontinent, Tectonophys, 644, 1–21, doi:10.1016/j.tecto.2015.01.007, 2015.

Singh, A., Eken, T., Mohanty, D. D., Saikia, D., Singh, C., and Kumar, M. R.: Significant seismic anisotropy beneath southern Tibet inferred from splitting of direct S-waves, Phys. Earth Planet. Inter., 250, 1–11, doi:10.1016/j.pepi.2015.11.001, 2016.

Sol, S., Meltzer, A., Bürgmann, R., Van der Hilst, R., King, R., Chen, Z., Koons, P., Lev, E., Liu, Y., Zeitler, P., et al.: Geodynamics of the southeastern Tibetan Plateau from seismic anisotropy and geodesy, Geology, 35, 563–566, doi:10.1130/G23408A.1, 2007.

5 Tapponnier, P., Peltzer, G., Le Dain, A., Armijo, R., and Cobbold, P.: Propagating extrusion tectonics in Asia: New insights from simple experiments with plasticine, Geology, 10, 611–616, doi:10.1130/0091-7613, 1982.

Tapponnier, P., Zhiqin, X., Roger, F., Meyer, B., Arnaud, N., Wittlinger, G., and Jingsui, Y.: Oblique stepwise rise and growth of the Tibet Plateau, Science, 294, 1671–1677, doi:10.1126/science.105978, 2001.

Tseng, T.-L., Chen, W.-P., and Nowack, R. L.: Northward thinning of Tibetan crust revealed by virtual seismic profiles, Geophys. Res. Lett.,
10 36, n/a–n/a, doi:10.1029/2009GL040457, l24304, 2009.

Van Hinsbergen, D. J., Lippert, P. C., Dupont-Nivet, G., McQuarrie, N., Doubrovine, P. V., Spakman, W., and Torsvik, T. H.: Greater India Basin hypothesis and a two-stage Cenozoic collision between India and Asia, Proceedings of the National Academy of Sciences, 109, 7659–7664, doi:10.1073/pnas.1117262109, 2012.

Vinnik, L. and Montagner, J.-P.: Shear wave splitting in the mantle Ps phases, Geophys. Res. Lett., 23, 2449–2452, doi:10.1029/96GL02263,
15 1996.

Vinnik, L., Kosarev, G., and Makeeva, L.: Lithosphere anisotropy from the observation of SKS and SKKS waves, Doklady Akademii Nauk SSSR, 278, 1335–1339, 1984.

Vinnik, L., Green, R., and Nicolaysen, L.: Recent deformations of the deep continental root beneath southern Africa, Nature, 375, 50–52, doi:10.1038/375050a0, 1995.

20 Vinnik, L., Singh, A., Kiselev, S., and Kumar, M. R.: Upper mantle beneath foothills of the western Himalaya: subducted lithospheric slab or a keel of the Indian shield?, Geophys. J. Int., 171, 1162–1171, doi:10.1111/j.1365-246X.2007.03577.x, 2007.

Vinnik, L. P., Makeyeva, L. I., Milev, A., and Usenko, A. Y.: Global patterns of azimuthal anisotropy and deformations in the continental mantle, Geophys. J. Int., 111, 433–447, doi:10.1111/j.1365-246X.1992.tb02102.x, 1992.

Wang, C., Chang, L., Lü, Z., Qin, J., Su, W., Silver, P., and Flesch, L.: Seismic anisotropy of upper mantle in eastern Tibetan Plateau and
25 related crust-mantle coupling pattern, Science in China Series D: Earth Sciences, 50, 1150–1160, doi:10.1007/s11430-007-0053-5, 2007.

Wang, C.-Y., Flesch, L. M., Silver, P. G., Chang, L.-J., and Chan, W. W.: Evidence for mechanically coupled lithosphere in central Asia and resulting implications, Geology, 36, 363–366, doi:10.1130/G24450A.1, 2008.

Wüstefeld, A. and Bokelmann, G.: Null detection in shear-wave splitting measurements, Bull. Seismol. Soc. Am., 97, 1204–1211, doi:10.1785/0120060190, 2007.

30 Wüstefeld, A., Bokelmann, G., Zaroli, C., and Barruol, G.: SplitLab: A shear-wave splitting environment in Matlab, CG, 34, 515–528, doi:10.1016/j.cageo.2007.08.002, 2008.

Yao, H., Beghein, C., and Van Der Hilst, R. D.: Surface wave array tomography in SE Tibet from ambient seismic noise and two-station analysis-II. Crustal and upper-mantle structure, Geophys. J. Int., 173, 205–219, doi:10.1111/j.1365-246X.2007.03696.x, 2008.

Yao, H., Van Der Hilst, R. D., and Montagner, J.-P.: Heterogeneity and anisotropy of the lithosphere of SE Tibet from surface wave array
35 tomography, JGR, 115, n/a–n/a, doi:10.1029/2009JB007142, 2010.

Yin, A. and Harrison, T. M.: Geologic Evolution of the Himalayan-Tibetan Orogen, Annual Rev. Earth Planet Sci., 28, 211 – 280, doi:10.1146/annurev.earth.28.1.211, 2000.

Zhang, P.-Z., Shen, Z., Wang, M., Gan, W., Bürgmann, R., Molnar, P., Wang, Q., Niu, Z., Sun, J., Wu, J., et al.: Continuous deformation of the Tibetan Plateau from global positioning system data, Geology, 32, 809–812, doi:10.1130/G20554.1, 2004.

Zhao, J., Yuan, X., Liu, H., Kumar, P., Pei, S., Kind, R., Zhang, Z., Teng, J., Ding, L., Gao, X., et al.: The boundary between the Indian and Asian tectonic plates below Tibet, Proceedings of the National Academy of Sciences, 107, 11 229–11 233, doi:10.1073/pnas.1001921107, 2010.

Zhao, J., Murodov, D., Huang, Y., Sun, Y., Pei, S., Liu, H., Zhang, H., Fu, Y., Wang, W., Cheng, H., et al.: Upper mantle deformation beneath central-southern Tibet revealed by shear wave splitting measurements, Tectonophys, 627, 135–140, doi:10.1016/j.tecto.2013.11.003, 2014.

Zhou, H. and Murphy, M. A.: Tomographic evidence for wholesale underthrusting of India beneath the entire Tibetan plateau, J. Asian Earth Sci., 25, 445 – 457, doi:10.1016/j.jseaes.2004.04.007, 2005.

Table 1. Obtained average splitting parameter (ϕ_s and δt_s) estimated from direct-S wave splitting measurement.

stations	latitude(°)	longitude(°)	ϕ_s (°)	δt_s(sec)	number of event at a station
ES01	31.26	92.09	73.9	1.5	31
ES02	31.00	92.54	75.7	1.5	26
ES03	30.75	92.86	81.7	1.2	16
ES04	30.65	93.25	91.5	1.2	11
ES05	31.68	92.40	71.2	1.1	14
ES07	31.48	93.70	93.8	1.0	15
ES08	31.28	93.84	106.3	0.9	12
ES09	31.91	93.06	81.5	1.1	15
ES10	31.84	93.79	103.1	1.0	19
ES11	31.91	94.14	96.2	1.2	25
ES12	31.59	94.71	101.3	1.2	28
ES13	31.54	95.28	88.5	1.4	15
ES14	31.25	95.90	102.9	1.2	24
ES15	31.19	96.50	104.2	1.0	9
ES16	31.18	97.02	117.0	1.4	1
ES17	31.27	97.55	135.4	1.0	11
ES18	31.30	97.96	122.0	0.8	2
ES19	30.81	95.71	106.6	1.5	9
ES20	30.73	96.10	108.0	0.9	1
ES22	30.81	96.70	110.0	0.9	1
ES23	30.69	97.26	96.2	1.0	16
ES24	30.50	97.14	106.0	1.1	3
ES25	30.12	97.30	121.1	0.9	10
ES26	29.96	97.51	142.2	1.0	3
ES27	29.64	97.90	130.0	1.1	1
ES29	30.01	96.69	84.0	1.1	16
ES30	29.32	97.19	110.8	1.1	7
ES31	29.51	96.76	82.4	1.2	16
ES32	29.76	96.10	103.0	1.4	2

stations	latitude(°)	longitude(°)	ϕ_s (°)	δt_s(sec)	number of event at a station
ES33	29.77	95.70	67.1	0.6	10
ES34	29.91	95.47	84.8	1.2	20
ES35	29.96	94.78	111.9	1.1	9
ES36	29.81	93.91	86.2	1.1	13
ES37	29.90	93.51	80.5	1.4	7
ES38	30.02	92.97	72.5	1.2	18
ES39	29.87	92.62	75.8	1.6	17
ES40	29.71	92.15	78.0	1.4	14
ES41	29.19	91.76	70.4	1.7	14
ES42	28.90	91.94	108.6	1.6	6
ES43	29.04	92.23	75.4	1.2	5
ES45	29.12	93.78	65.8	1.3	5
ES46	29.25	94.26	89.2	1.1	4
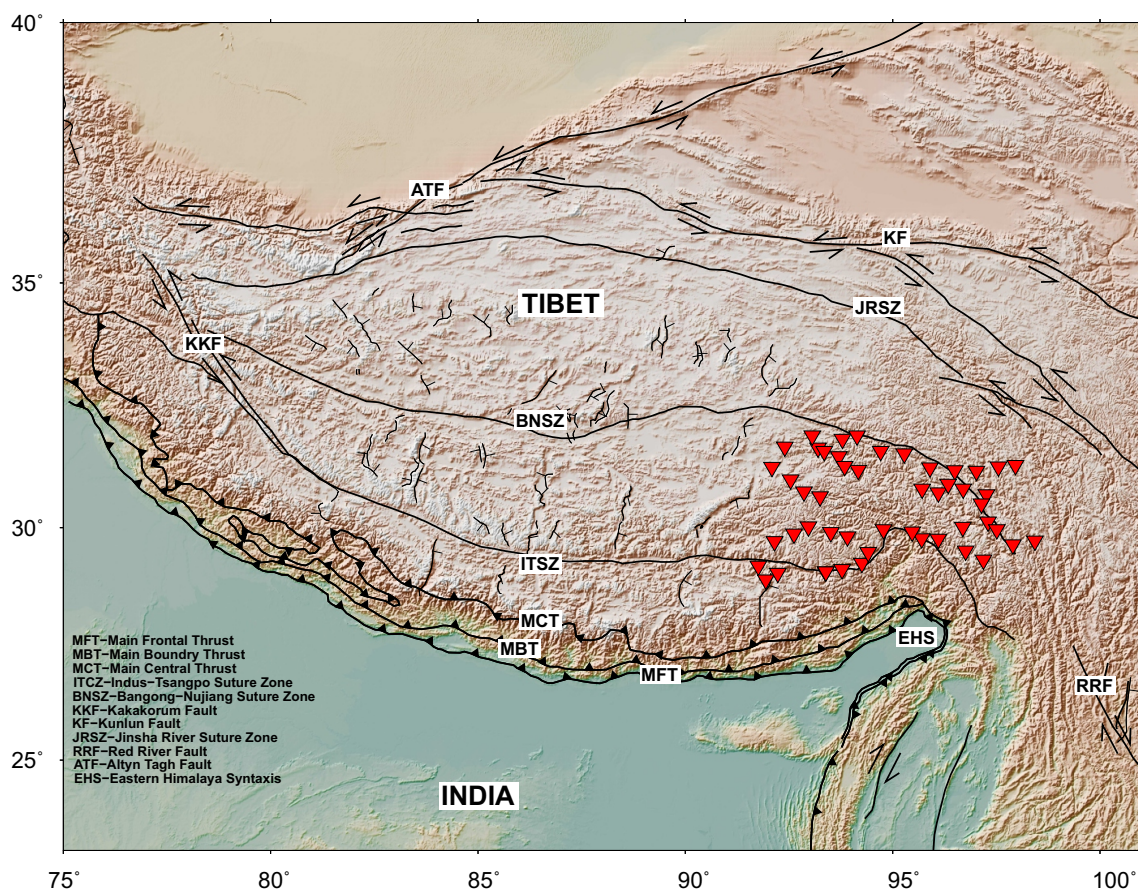
Figure 1. Tectonic and topographic map of Himalaya and Tibet. Red triangles represent the broadband seismic stations of XE network from the study region.
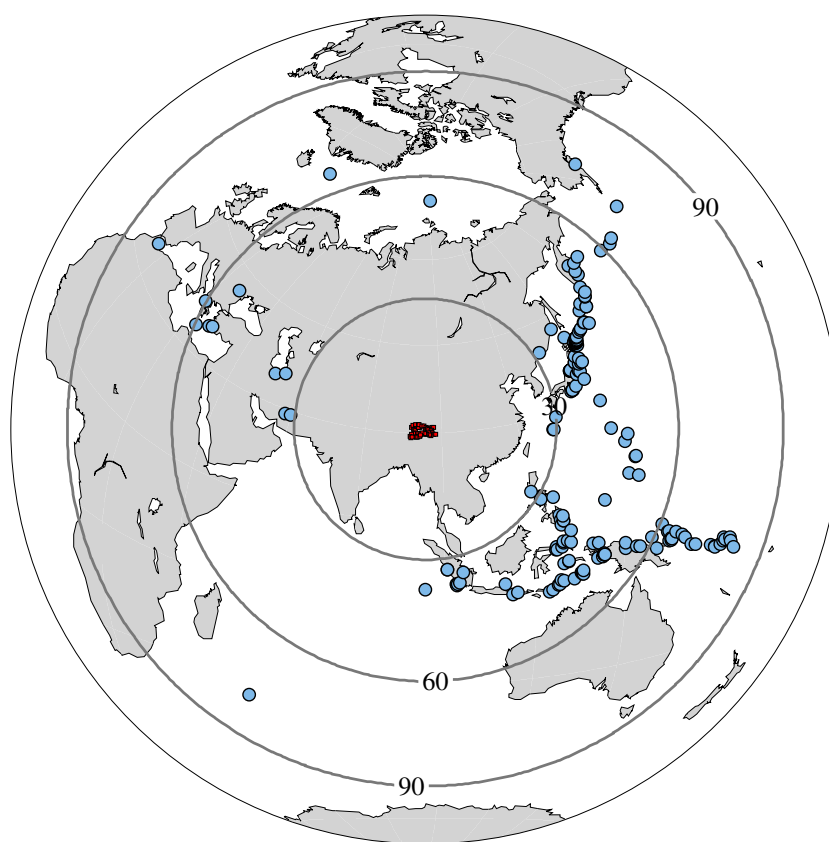
Figure 2. Epicentral distribution of the earthquake events used in the study (30°-90°). Rectangles denote the location of seismic stations.
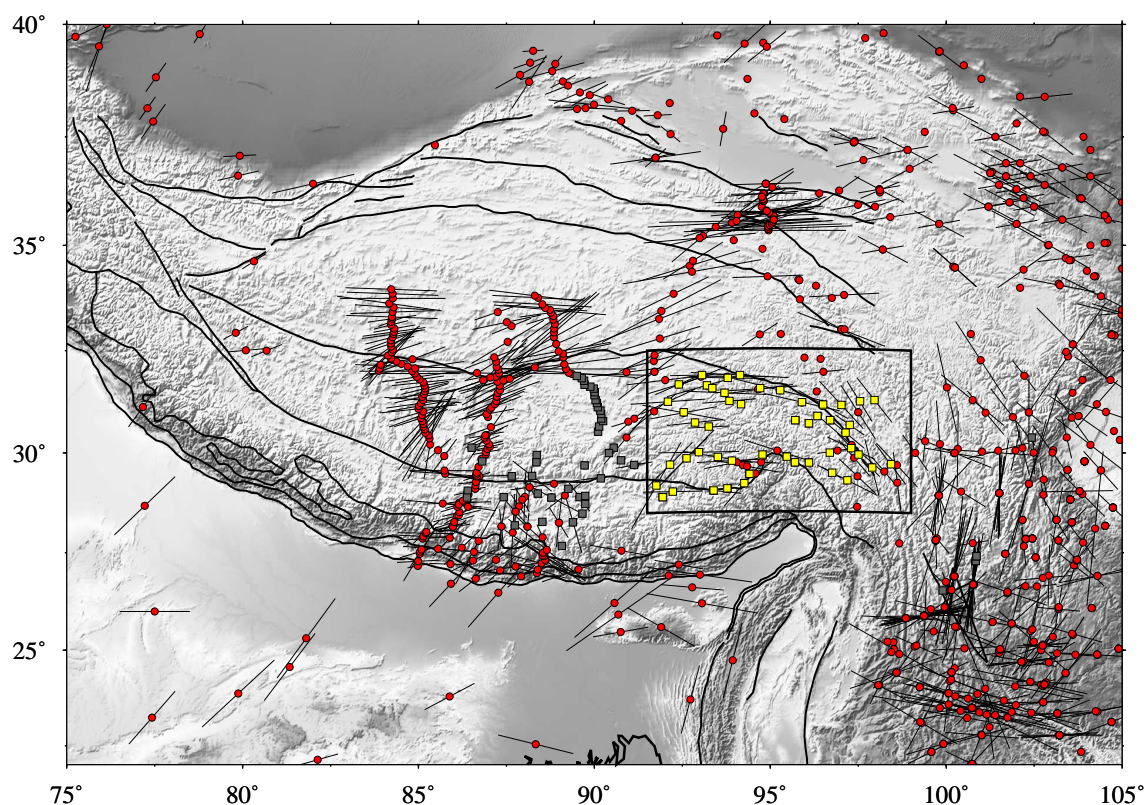
Figure 3. Earlier SKS/SKKS measurements in the area (Sol et al., 2007; Wüstefeld et al., 2008). The length of line at each seismic station represents the delay time (δt_s) and their orientation denotes the fast polarization direction (ϕ_s). For clarity, the seismic stations used in the present study are shown by yellow filled rectangles along with the SKS splitting measurements of Sol et al. (2007). Seismic stations where null or negligible anisotropy is reported in earlier studies (see Wüstefeld et al., 2008) are shown by gray filled rectangles.
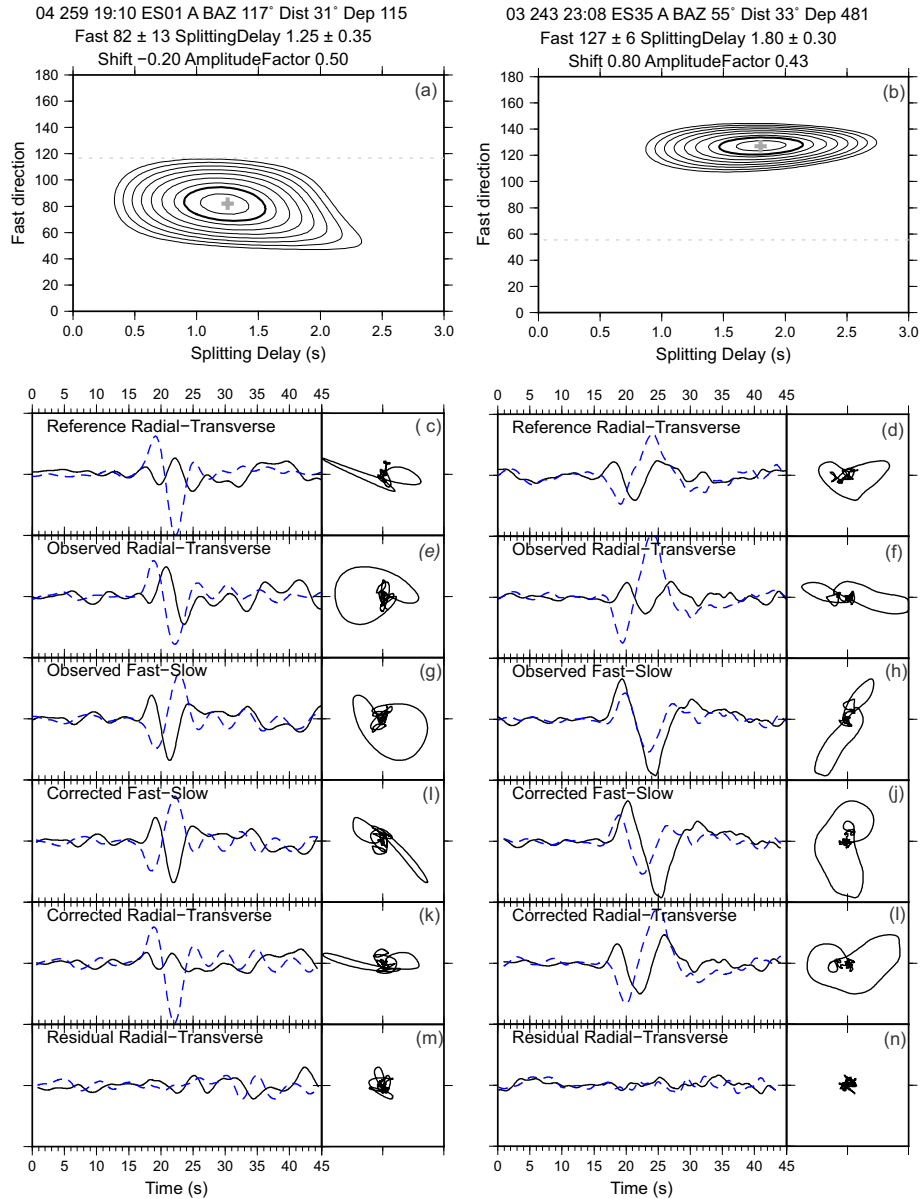
Figure 4. Examples of the direct-S waves splitting measurements based on the Reference Station Technique at stations ES01 and ES35. Figures on the left panel represents the splitting measurement recorded at station pair ES03 (reference station) - ES01 (target station) and on the right panel represent the splitting measurement recorded at station pair ES16 (reference station) - ES35 (target station). (a) Misfit surface with splitting parameter $82° \pm 13°$ and 1.25 ± 0.35 s. (c) signal at reference station (ES03) with receiver side correction. (e) signal at target station (ES01). (g) fast and slow component after rotating signal at target station (ES01) using ϕ ($82°$). (i)fast and slow component corrected for δt (1.25s). (k) corrected radial and transverse components at target station (ES01) using optimum ϕ and δt and isotropic delay (-0.2s). (m) residual trace. Figures on the right panel follow the similar order and explanation.
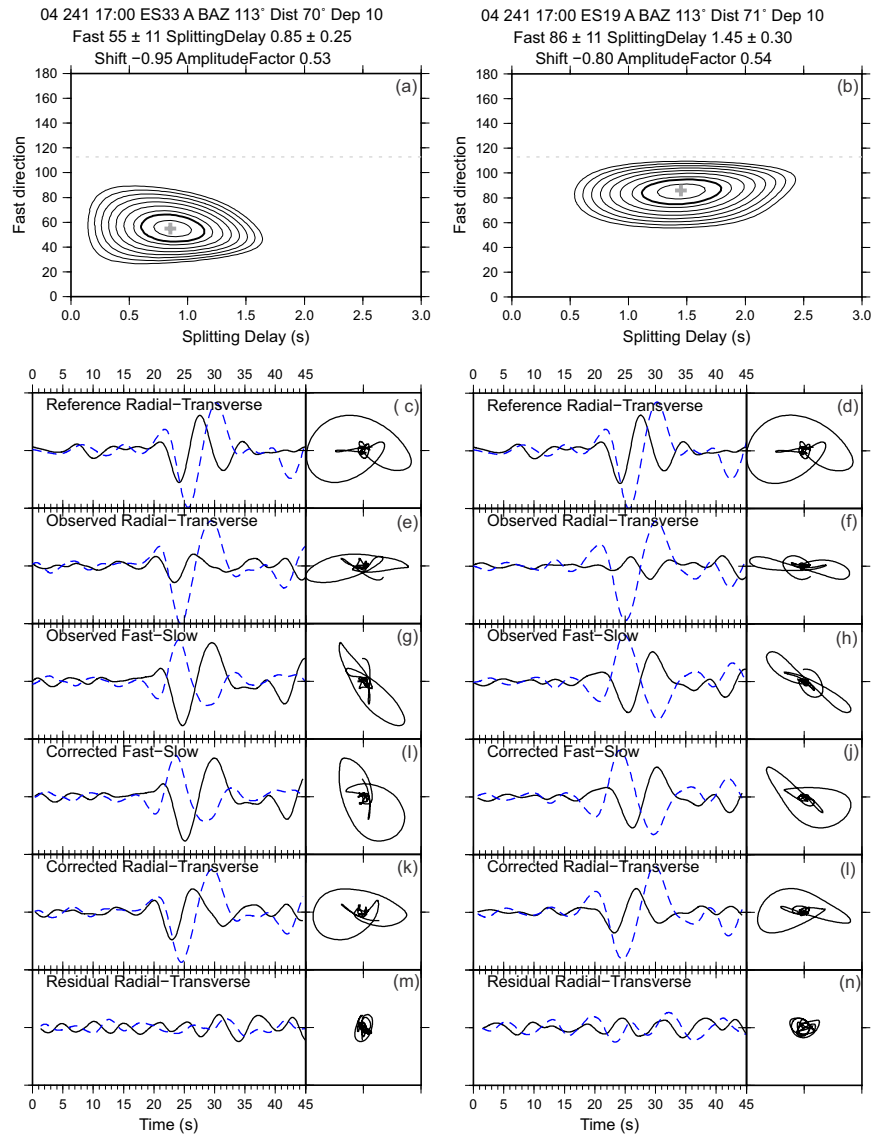
Figure 5. Examples of the direct-S waves splitting measurements based on the Reference Station Technique at stations ES33 and ES19, where previously null anisotropy were obtained by using SKS splitting measurement (Sol et al., 2007). Figures on the left panel represent the splitting measurement recorded at station pair ES12 (reference station) - ES33 (target station) and on the right panel represent the splitting measurement recorded at station pair ES12 (reference station) - ES19 (target station). Explanation for each panel is same as in the Figure 4.
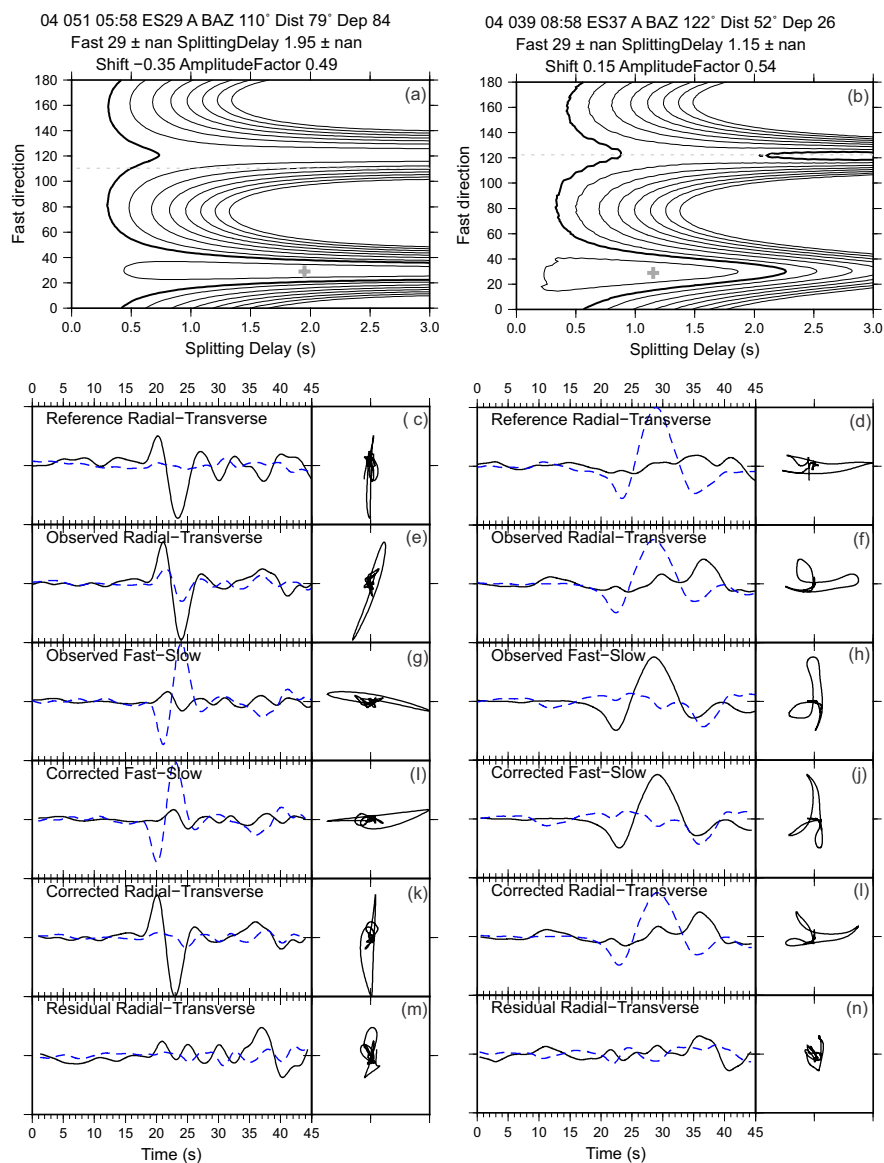
Figure 6. Examples of the null anisotropic measurement based on Reference Station Technique at stations ES29 and ES37. Figures on the left panel represent the splitting measurement recorded at station pair ES27 (reference station) - ES29 (target station) and on the right panel represent the splitting measurement recorded at station pair ES05 (reference station) - ES37 (target station). Explanation for each panel is same as in the figure 4.
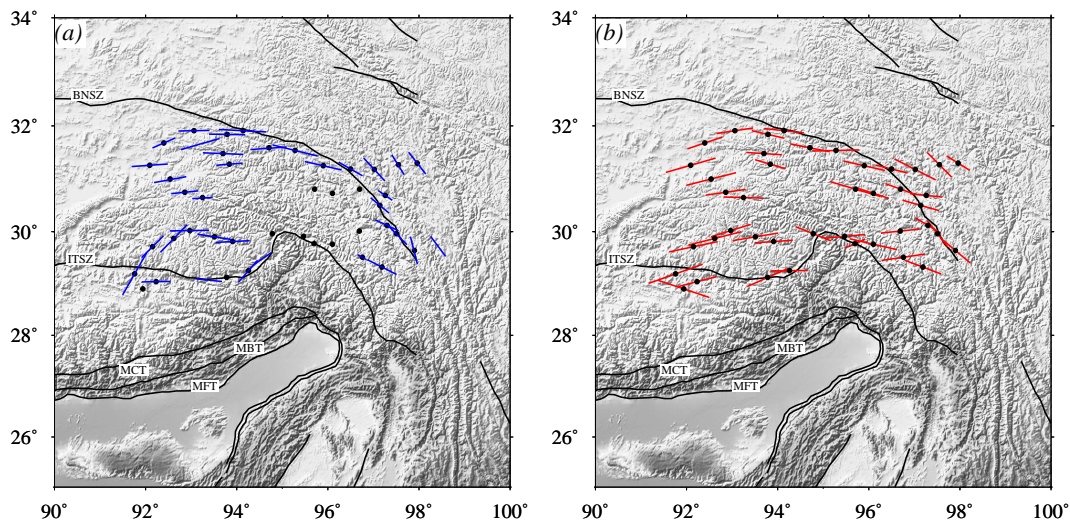
Figure 7. The tectonic and topographic map of the Southeastern Tibetan region that represents the station average splitting parameters: (a) the previous splitting measurements performed by Sol et al. (2007), and (b) the direct S-waves ?derived splitting measurements (this study). The length of the the solid bars in each panel indicates the strength of anisotropy and scaled by station averaged splitting time delays. Azimuth of the solid bars indicates the orientation of fast shear waves or fast polarization direction (FPD). Black circle denotes our seismic station of the study area, red line representing our splitting measurement of the direct S phase, and blue line denote the splitting of the SKS phase (MFT: Main Frontal Thrust; MBT: Main Boundary Thrust; MCT: Main Central Thrust; ITCZ: Indus-Tsangpo Suture Zone; BNSZ: Bangong-Nujiang Suture Zone).
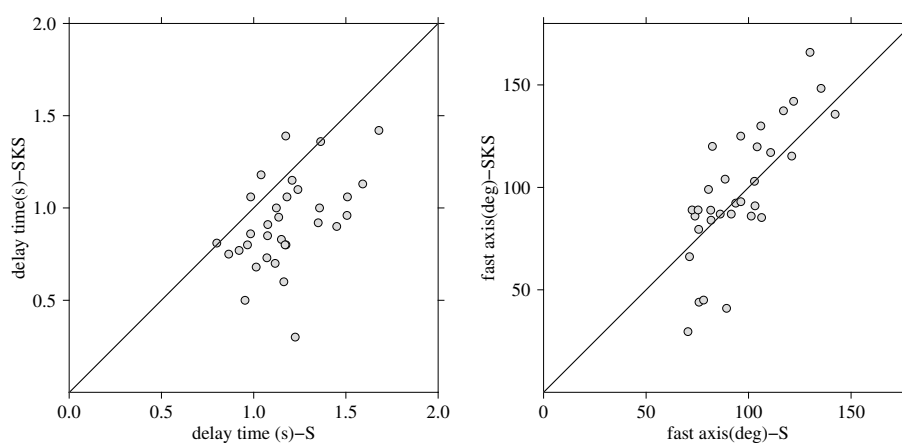
Figure 8. Scatter plot that shows the comparison between station average SKS-derived and S-derived splitting parameters (FPD and time delays). Average SKS splitting parameters are taken from Sol et al. (2007).
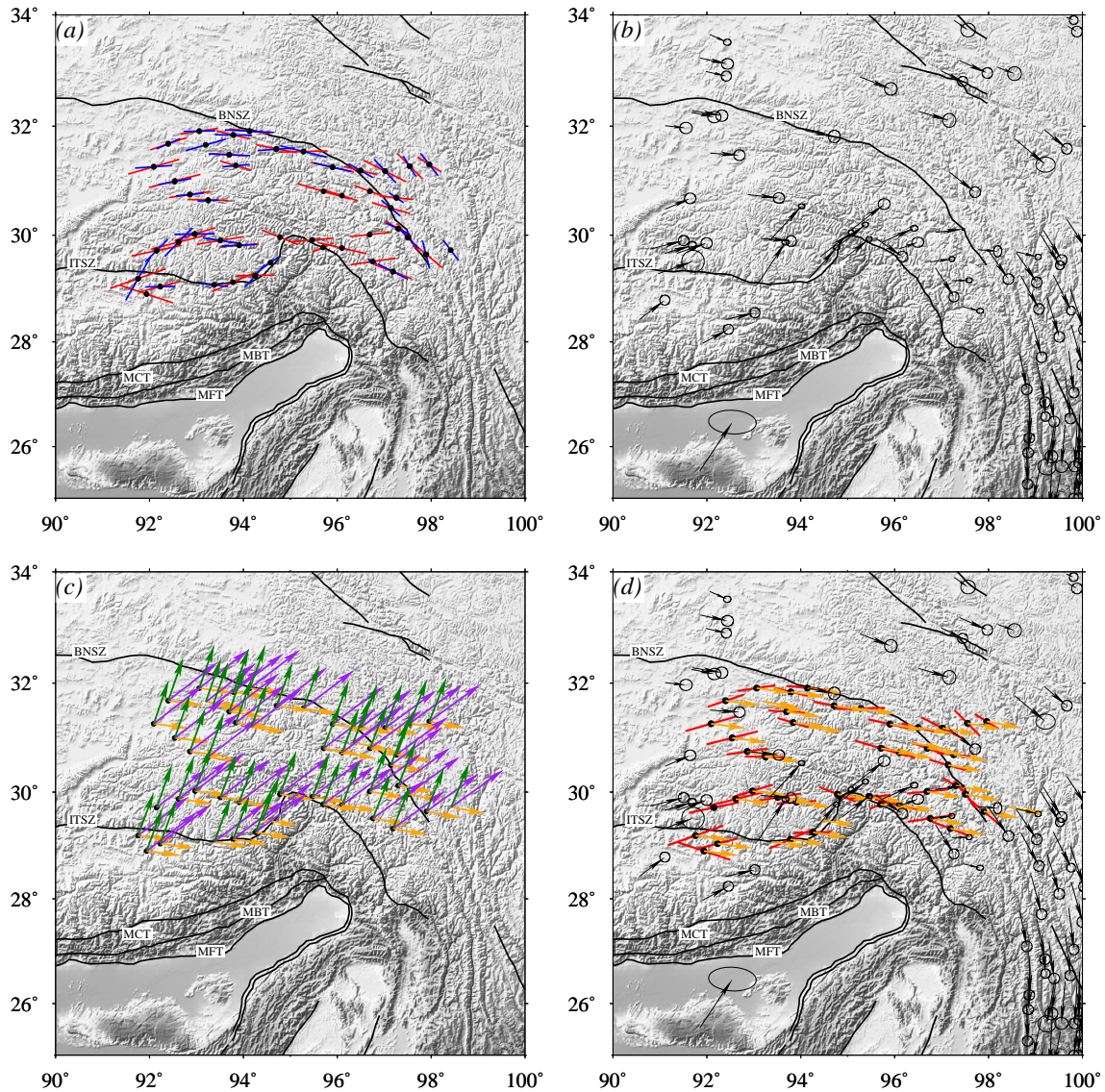
Figure 9. Lateral variation of anisotropic, geodetic, absolute plate motion data shown over topographic and tectonic features of the study area. (a) Map view comparison between the splitting measurement inferred from direct-S waves (this study shown by red bars) and SKS phase (Sol et al., 2007, in blue bars) measurements. (b) The Global Positioning System (GPS) velocity (mm/yr) vectors (black arrows) around SE Tibetan region calculated with respect to the South China reference frame and stable Eurasia. GPS data is compiled from several studies including Chen et al. (2000); Zhang et al. (2004); Shen et al. (2005); Sol et al. (2007). (c) Absolute plate motion (APM) velocities calculated from https://www.unavco.org/software/geodetic-utilities/plate-motion-calculator/platemotion-calculator.html by using GSRM v1.2 (2004) model of Kreemer et al. (2003) Note that arrows in orange, green, and purple represent the APM velocities of the Eurasian plate in no net rotation frame, of the Indian plate with respect to the Eurasian plate, and the motion of the Indian plate in no net rotation frame, respectively. (d) Map view comparisons of the station (black circle) average direct S-waves derived splitting parameters with GPS velocity (black arrow) and APM (orange arrow) vectors. Abbreviations on the maps correspond: MFT: Main Frontal Thrust; MBT: Main Boundary Thrust; MCT: Main Central Thrust; ITCZ: Indus-Tsangpo Suture Zone; BNSZ: Bangong-Nujiang Suture Zone; JRSZ: Jinsa River Suture Zone.